

Observation of Dynamical Ordering in a Confined Wigner Crystal

P. Glasson, V. Dotsenko, P. Fozooni, M.J. Lea, W. Bailey, and G. Papageorgiou

Department of Physics, Royal Holloway, University of London, Egham, Surrey TW20 0EX, United Kingdom

S. E. Andresen and A. Kristensen*

The Niels Bohr Institute fAPG, University of Copenhagen, Copenhagen, Denmark

(Received 16 March 2001; published 5 October 2001)

We present measurements of the conduction of nondegenerate free electrons along a low-dimensional channel at low temperatures, using surface-state electrons on liquid helium in novel microelectronic devices. Above 1 K, the electrons form an ideal classical Drude conductor. Below 1 K, Coulomb interactions produce electronic spatial order, leading to strong non-Ohmic effects and negative differential conductivity. Evidence is presented for self-organized current filaments in the channel, created by a nonequilibrium phase transition. Periodic conductance oscillations suggest an anisotropic spatial order with lines of electrons along the channel edges.

DOI: 10.1103/PhysRevLett.87.176802

PACS numbers: 73.20.-r, 73.50.Fq

The conductivity and ground state of two-dimensional (2D) electrons are strongly affected by electron-electron interactions [1] in semiconductors (including organic semiconductors [2]) and in surface-state electrons on cryogenic substrates [3]. Examples are the fractional quantum Hall effect [2], the unexpected metal-insulator transition [4] in Si and GaAs, and the crystallization of electrons on liquid helium [3]. In the low-density limit, or in very high magnetic fields, the theoretical ground state is the classical 2D Wigner crystal. In semiconductors, material defects can produce carrier localization to give a statically pinned crystal [5], or a Wigner glass, whereas a moving 2D crystal on superfluid helium can be dynamically pinned [6] to the surface vibrations, or ripples. Pinning produces a characteristic nonlinear conductivity [7]. We report new experiments, dynamically probing a classical Wigner electron solid that is laterally confined within a narrow microchannel [8,9] on helium. Moving the crystal along the channel generates a new, dynamically ordered, striped phase of current filaments. As the driving field increases, a nonequilibrium phase transition occurs in which a central crystalline region coexists with edge currents consisting of discrete, and mobile, lines of electrons.

Surface-state electrons on liquid helium are attracted by a weak positive image charge in the liquid and are held by a vertical electric field E_z . Below 2 K, they are in the lowest energy level for vertical motion, “floating” about 11 nm above the surface [3].

We have fabricated novel microelectronic devices to create microchannels [9] 16 μm wide with a depth $d = 1.6 \mu\text{m}$ (Fig. 1). These are placed above the free surface of superfluid helium, filled by capillary rise, and are charged with electrons by thermionic emission from a filament. Electrons above the metallic guard electrode drain away through the thin van der Waals helium film. The electrons are controlled by dc potentials on the underlying source, drain, and gate electrodes, giving a three-terminal device. An audio frequency ($\omega/2\pi = 5\text{--}20$ kHz) voltage

V_d is applied to the source electrode and drives an ac source-drain current I via capacitive coupling to the electrons, Fig. 1(c) [10]. The magnitude of the capacitive current $|I|$ enables us to calculate the area of the electron sheet and shows that the effective width of the

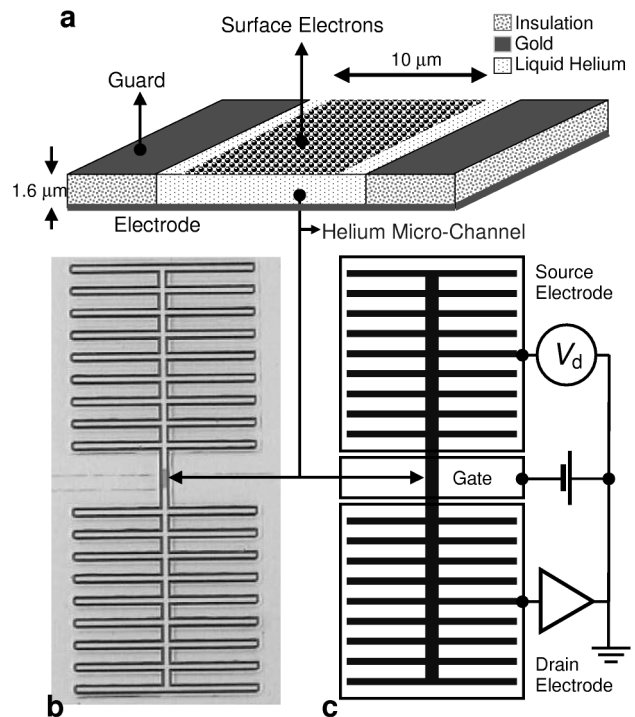


FIG. 1. The new microelectronic devices. (a) Schematic of an electronic microchannel: two Au layers were evaporated on a semi-insulating GaAs wafer, separated by 1.2 μm of hard-baked resist, using e -beam lithography. The lower gold layer forms a source, drain, or gate electrode, while the upper layer is a guard. (b) Photograph of the device: the side channels increase the capacitance of the source and drain electrodes. The dimensions of the device are $428 \mu\text{m} \times 952 \mu\text{m}$. (c) Circuit diagram: the source, gate, and drain electrodes are capacitively coupled to the electrons (shaded areas).

conducting channels is $W \approx 10 \mu\text{m}$. The average inter-electron separation is typically $\approx 0.5 \mu\text{m}$ with N (≈ 20) electron spacings across the channel. A negative gate voltage ΔV_g cuts off the current by depleting the electron density over the gate electrode, as in a field effect transistor. The maximum 2D electron concentration $n \text{ m}^{-2}$ can be determined from the expression for a capacitance $n = \epsilon\epsilon_0\Delta V_g/ed$.

The effective resistance per square, or resistivity, $\rho(T)$ of the 2D electron sheet in the channel is found from the phase shift ϕ and is plotted versus the temperature T in Fig. 2. The resistance above 1 K is Ohmic, independent of the excitation voltage and the electron drift velocity. Electrons are scattered by ^4He vapor atoms and the resistance falls as the vapor pressure decreases, Fig. 2(a). The solid line shows a theoretical fit [11] to the data. The electrons form a classical conductor (i.e., not Fermi degenerate), as originally proposed by Drude [12], but in two dimensions.

A striking change occurs below 1 K, as the effective resistance unexpectedly rises, Fig. 2(b), and becomes strongly non-Ohmic, increasing with the excitation voltage. It reaches a maximum close to the theoretical melting temperature of the Wigner crystal at $T_m = 0.225 \times 10^{-6}n^{1/2}$ corresponding to the maximum density. We associate this nonlinearity with the transition from an isotropic electron fluid at high temperatures to a spatially ordered phase near T_m . The amplitude dependence of the current I versus V_d at 0.52 K, below T_m , is shown explicitly in Fig. 3(a). The capacitive component, $\text{Im}(I)$, increases with drive, while the resistive component, $\text{Re}(I)$, shows a distinctive nonlinear behavior. The in-plane electric field amplitude E in the central channel, and hence the force $F = -eE$ felt by the electrons, is $E \approx \phi V_d/L \approx \text{Re}(I)V_d/|I|L$, where L is a characteristic length for the device ($395 \mu\text{m}$). This field is shown in Fig. 3(b) versus the electron drift velocity amplitude $v = \sqrt{2}|I|/neW$.

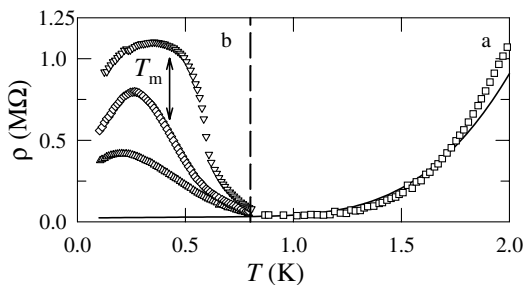


FIG. 2. Effective resistivity $\rho(T)$ of the electron sheet. The electrical resistance $R = K\rho$ (K is a geometrical constant) of the device is measured from the phase shift $\phi = \text{Re}(I)/\text{Im}(I) \propto \omega CR$, where C is the source-drain capacitance and $\text{Re}(I)$ and $\text{Im}(I)$ are the resistive and capacitive components of the ac source-drain current I . (a) $\rho(T)$ above 0.8 K (\square) for $n = 5.1 \times 10^{12} \text{ m}^{-2}$. The line shows theoretical calculations. (b) The effective $\rho(T)$ below 0.8 K for electron velocity amplitudes of 16 (Δ), 31 (\diamond), and 64 (∇) m/s, for $n = 3.5 \times 10^{12} \text{ m}^{-2}$ ($T_m = 0.42 \text{ K}$).

This is the ac force-velocity characteristic $F(v)$ for electrons in the channel. Measurements at different frequencies clearly show that the nonlinearity depends on the electron current density, or electron velocity, and not on the applied voltage.

The novel significant feature is that this field is almost constant at $E = E_{\text{max}}$ for $v > 30 \text{ m/s}$. The force remains the same as the velocity increases. The effective resistance of the device $R \propto E/V_d$ then decreases as V_d^{-1} . A linear, Ohmic region occurs only at velocities $< 7 \text{ m/s}$ [Fig. 3(b) inset]. This velocity value indicates that surface vibrations, or ripples, on the helium are responsible for the nonlinearity. Measurements [6,7] of the magnetoconductivity of the 2D electron solid on bulk helium show a sharp increase in the resistive force as the drift velocity of the crystal approaches a critical velocity v_1 . This is due to the Bragg-Cerenkov radiation [13] of coherent ripples, whose wavelength equals the electron lattice spacing (i.e., the ripplon wave vector $\mathbf{q} = \mathbf{G}_1$, the first reciprocal lattice vector of the crystal). As the crystal drift velocity \mathbf{v} approaches the phase velocity of these ripples, $v_1 = 4.03 \times 10^{-3}n^{1/4} \text{ m/s}$, the drag force diverges as $\mathbf{F}(\mathbf{v}) \propto -\mathbf{v}/(1 - v/v_1)^{1-\beta(\mathbf{G})}$, where $\beta(\mathbf{G}) \approx 0$ at low temperatures [13]. This force dynamically pins the moving Wigner crystal at $v \leq v_1$. The crystalline order produces nonlinear conductivity via coherent ripplon scattering. For the electron density in Fig. 3, $v_1 = 7.1 \text{ m/s}$, close to the end

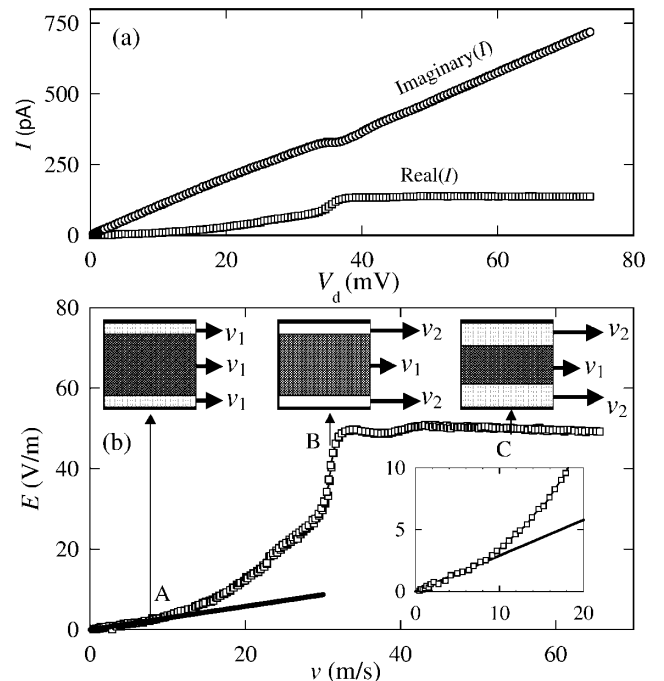


FIG. 3. Nonlinear response. (a) The capacitive $\text{Im}(I)$ and resistive $\text{Re}(I)$ components versus rms drive voltage at 0.52 K for $n = 9.8 \times 10^{12} \text{ m}^{-2}$. (b) The in-plane electric field $E(v)$ versus the electron drift velocity amplitude v (field-velocity characteristic). The inset shows the Ohmic region at low velocities with a mobility of $3.0 \text{ m}^2/\text{Vs}$. The model diagrams show the current filaments at points A, B, and C on the characteristic.

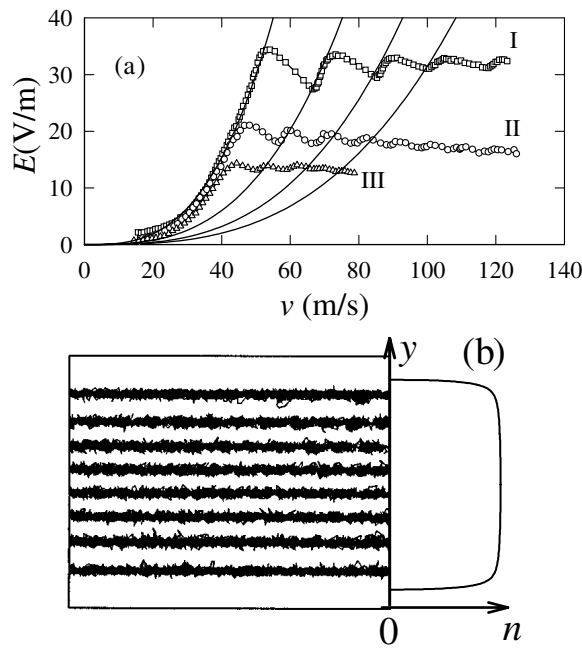


FIG. 4. Oscillations in the electronic response. (a) The field-velocity characteristic $E(v)$ for electrode voltages of 1.8 (data I), 1.2 (II), and 0.8 V (III), relative to the guard potential, for $n = 3.0 \times 10^{12} \text{ m}^{-2}$. The lines are guides to the eye to show the “switching” of the characteristic. (b) Molecular dynamics simulations [22] show the trajectories of electrons in a channel just above the melting temperature. The solid line shows a calculated average electron density profile $n(y)$ across the channel.

of the Ohmic region, indicating that the same mechanism applies here.

The constant field at higher velocities follows directly from this nonlinear interaction. Above some critical field E_{max} , at $v \approx v_1$, the ordered electrons decouple from the ripples and the drag force $F(v)$ decreases, producing negative differential conductivity [14]. For velocities up to v_1 , the resistive force ($= eE$) increases. But for $v > v_1$, the system becomes unstable and current filaments can form with different drift velocities. The average velocity $\bar{v} = \alpha v_1 + (1 - \alpha)v_2$, where a fraction α of the electrons are *dynamically pinned* to the ripples at a velocity v_1 and a fraction $(1 - \alpha)$ are *decoupled* from the ripples and move at a velocity v_2 , all in a field E_{max} . For the decoupled electrons, with $v \gg v_1$, $v = \mu E$ with a mobility $\mu = v_2/E_{\text{max}}$.

But the electron density varies across the channels, decreasing to zero at the edges [see Fig. 4(b)]. Hence both v_1 and E_{max} will tend to zero at the channel edges. We present a simple model, with uniform central and edge filaments, in which an edge current fraction $(1 - \alpha_0)$ can be decoupled even for $\bar{v} < v_1$ and which has a mobility μ for all velocities.

Because of the high-impedance capacitive coupling, the applied voltage V_d acts as a current source, with $\bar{v} \propto V_d$. On this model, \bar{v} increases linearly up to v_1 [point A in Fig. 3(b)]. The field, and the edge current velocity,

then increase further while keeping the central pinned region at v_1 , up to the field E_{max} and an edge velocity v_2 (point B). For higher average velocities \bar{v} , the filament velocities remain constant, but α now decreases, as the edge filaments grow at the expense of the center (point C). The edge (fast) and central (slow) current filaments coexist in the same electric field E_{max} . The critical average electron velocity, \bar{v}_{crit} , at which E_{max} is first reached, depends on the value α_0 in the low velocity limit:

$$\bar{v}_{\text{crit}} = v_1 + (1 - \alpha_0)(v_2 - v_1). \quad (1)$$

Hence $\bar{v}_{\text{crit}} > v_1$, as observed [$\bar{v}_{\text{crit}} = 31 \text{ m/s}$ in Fig. 3(b)], if $\alpha_0 < 1$. The edges, with lower electron density, and edge currents play an important role, as they do in other low-dimensional conductors such as GaAs heterostructures.

The constant field E_{max} is the signature of a nonequilibrium phase transition [14,15], in which two current filament states coexist. It is analogous to the constant pressure region on the P - V isotherms of a gas-liquid mixture, with the van der Waals equation being equivalent to the $E(v)$ characteristic.

The magnitude of E_{max} is related to the coherent Bragg enhancement of the ripplon scattering by the ordered electrons. According to Rubo [16] and Vinen [17], the maximum force per electron on the Wigner crystal, expressed as an electric field, can be written as $eE_{\text{max}} = ne^2 E_z^2 \xi / 2\tau$, where τ is the surface tension of the helium and ξ is an effective correlation length of the 2D electrons. The gradual decrease of the nonlinearity above T_m shows that this correlation length decreases in a continuous transition as the temperature rises, in the strongly correlated electron fluid (or Wigner liquid), confirming previous conclusions from the magnetoconductivity [18] in this region. We find experimentally that E_{max} increases with the pressing field E_z [see Fig. 4(a)], confirming the role of the ripples. Bragg scattering produces a strong force, compared to the normal ripplon scattering in the electron crystal and electron fluid [19]. The maximum power dissipation in our experiments is typically $< 10 \text{ pW}$. We estimate that the temperature rise due to Joule heating of the electrons is less than 5 mK at 0.5 K for 10 pW dissipation.

Other nonlinear effects [20] would produce forces that decrease with increasing drift velocity. Nonlinear effects are not observed in dielectric channels containing a single line of electrons on helium [21].

We also find evidence for a further ordered state within the edge currents themselves. Periodic oscillations in the maximum field E_{max} at electronic velocities $\bar{v}_{\text{osc}} > \bar{v}_{\text{crit}}$ are shown in Fig. 3(b) and more clearly in Fig. 4(a). These oscillations are equally spaced in electron velocity with a periodicity $\Delta \bar{v}_{\text{osc}}$, and are shown for several values of the dc electrode potentials (and hence the pressing field E_z) in Fig. 4(a). They are most pronounced just above the theoretical melting temperature T_m .

Molecular dynamics computer simulations by Bajaj and Mehrotra [22] provide a natural explanation. They showed that classical electrons in a microchannel exhibit anisotropic spatial order above T_m , with the electrons forming mobile discrete lines along the channel as in Fig. 4(b). In the present context, as the electron velocity increases, the edge region would increase by discrete lines of electrons, giving rise to periodic oscillations in the conductance and $E(v)$, with a period $\Delta\bar{v}_{\text{osc}}$. Using the model above, we put $\alpha = (1 - N_{\text{edge}})/N$, where N_{edge} is the number of edge electron lines. The critical average velocity, Eq. (1), becomes $\bar{v}_{\text{crit}} = (1 - N_{\text{edge}}/N)v_1 + (N_{\text{edge}}/N)v_2$. If α decreases in discrete increments by $\Delta\alpha = -1/N$, a series of critical velocities will occur with a spacing $\Delta\bar{v}_{\text{osc}} = (v_2 - v_1)/N = (\mu E_{\text{max}} - v_1)/N$.

The data in Fig. 4(a) (data set I) gives $v_1 = 7.1$, $v_2 = 310$ m/s, $N = 18$ with an initial value of $\alpha_0 \approx 0.84$. As the average electron velocity is increased, the $E(v)$ curve “switches” between discrete characteristics, as suggested by the lines in Fig. 4(a), whenever the driving field reaches the critical value E_{max} [23]. Note that $\Delta\bar{v}_{\text{osc}} \propto E_{\text{max}}$ for the three data sets, giving a mobility of ≈ 8 m²/V s. At lower temperatures, down to 0.06 K $\ll T_m$, irregular jumps in resistance are observed, as often found in current filaments or field domains in semiconductors [14] when the domain structure changes.

These experiments show that the dynamics of an electronic microchannel of nondegenerate electrons reveal a wide range of new phenomena at low temperatures, due to strong Coulomb interactions. We have demonstrated the use of gated electronic devices using microchannels of electrons on helium. Electrons in similar structures could form quantum bits or qubits in a putative quantum computer [24].

We thank M. I. Dykman and Y. G. Rubo for theoretical discussions and F. Greenough, A. K. Betts, and others for technical support. The work was supported by the EPSRC, the Danish Technical Research Council (Grant No. 9701490), INTAS, and Royal Holloway. The electrode structures were produced at the III-IV NANOLAB, operated jointly by Research Center COM and the Niels Bohr Institute.

*Present address: Mikroelektronik Centret (MIC), Oersteds Plads, DTU, DK-2800 Kgs.Lyngby, Denmark.

- [1] A. Isahara, *Solid State Phys.* **42**, 271 (1989).
- [2] J. H. Schon, C. Kloc, and B. Batlogg, *Science* **288**, 2338 (2000).
- [3] For a collection of review articles, see *Two-Dimensional Electrons on Cryogenic Substrates*, edited by E. Andrei (Kluwer Academic Press, Dordrecht, 1997).
- [4] M. P. Sarachik and S. V. Kravchenko, *Phys. Status Solidi B* **218**, 237 (2000).
- [5] C. C. Li, J. Yoon, L. W. Engel, D. Shahar, D. C. Tsui, and M. Shayegan, *Phys. Rev. B* **61**, 10 905 (2000).
- [6] A. Kristensen *et al.*, *Phys. Rev. Lett.* **77**, 1350 (1996).
- [7] K. Shirahama and K. Kono, *Phys. Rev. Lett.* **74**, 781 (1995).
- [8] D. Marty, *J. Phys. C* **19**, 6097 (1986).
- [9] P. Glasson *et al.*, *Physica (Amsterdam)* **284B**, 1916 (2000).
- [10] The capacitance of the electron sheet to the guard electrode is only 2.4% of the capacitance to the source and drain electrodes.
- [11] M. Saitoh, *J. Phys. Soc. Jpn.* **42**, 201 (1977).
- [12] P. Drude, *Ann. Phys. (Leipzig)* **1**, 566 (1900).
- [13] M. I. Dykman and Yuri G. Rubo, *Phys. Rev. Lett.* **78**, 4813 (1997).
- [14] *Nonlinear Dynamics in Solids*, edited by H. Thomas (Springer-Verlag, Berlin, 1992). The nonlinearity is “S-shaped” (SNDC), when plotted as a conventional I - V characteristic with $v \equiv I$ and $F(v) \equiv V$, which can be unstable to the formation of current filaments.
- [15] M. Lehr *et al.*, *Phys. Rev. B* **42**, 9019 (1990).
- [16] Y. G. Rubo (private communication).
- [17] W. F. Vinen, *J. Phys. Condens. Matter* **48**, 9709 (1999).
- [18] K. Djerfi *et al.*, *Phys. Rev. Lett.* **80**, 806 (1998).
- [19] R. Mehrotra *et al.*, *Phys. Rev. B* **29**, 5239 (1984).
- [20] S. S. Sokolov, G. Q. Hai, and N. Studart, *Phys. Rev. B* **51**, 5977 (1995).
- [21] Y. Z. Kovdrya, V. A. Nikolaenko, and S. P. Gladchenko, *Physica (Amsterdam)* **284B**, 168 (2000).
- [22] K. M. S. Bajaj and R. Mehrotra, *Physica (Amsterdam)* **194B-196B**, 1235 (1994).
- [23] Alternative explanations for these oscillations, based on Bragg-Cerenkov peaks from higher order reciprocal lattice vectors, or on the periodic structure of the source and drain electrodes, predict an irregular crystallographic sequence or $v_{\text{osc}}/v_{\text{crit}} = 1, 9/8, 9/7, 9/6, 9/5, 9/4, 9/3, 9/2$, and 9 from the nine side channels. Neither sequence is observed. Also Δv_{osc} would be independent of E_z [see Fig. 4(b)].
- [24] P. M. Platzman and M. I. Dykman, *Science* **284**, 1967 (1999); M. I. Dykman and P. M. Platzman, *Fortschr. Phys.* **48**, 1095 (2000); M. J. Lea, P. G. Frayne, and Y. Mukharsky, *Fortschr. Phys.* **48**, 1109 (2000).